CHEMISTRY OF MATERIALS

pubs.acs.org/cm

Article

Aqueous Processing and Spray Deposition of Polymer-Wrapped Tin-Doped Indium Oxide Nanocrystals as Electrochromic Thin Films

Anthony Maho,[#] Camila A. Saez Cabezas,[#] Kendall A. Meyertons, Lauren C. Reimnitz, Swagat Sahu, Brett A. Helms, and Delia J. Milliron*

Cite This: *Chem. Mater.* 2020, 32, 8401−8411

Read Online

ACCESS | Metrics & More | Article Recommendations | Supporting Information

ABSTRACT: Plasmonic metal oxide nanocrystals are interesting electrochromic materials because they display high modulation of infrared light, fast switching kinetics, and durability. Nanocrystals facilitate solution-based and high-throughput deposition, but typically require handling hazardous nonaqueous solvents and further processing of the as-deposited film with energy-intensive or chemical treatments. We report on a method to produce aqueous dispersions of tin-doped indium oxide (ITO) by refunctionalizing the nanocrystal surface, previously stripped of its native hydrophobic ligands, with a hydrophilic poly(acrylic acid) polymer featuring a low density of methoxy-terminated poly(ethylene oxide) grafts (PAA-mPEO$_4$). To determine conditions favoring the adsorption of PAA-mPEO$_4$ on ITO, we varied the pH and chemical species present in the exchange solution. The extent of polymer wrapping on the nanocrystal surface can be tuned as a function of the pH to prevent aggregation in solution and deposit uniform, smooth, and optical quality spray coated thin films. We demonstrate the utility of polymer-wrapped ITO nanocrystal thin films as an electrochromic material and achieve fast, stable, and reversible near-infrared modulation without the need to remove the polymer after deposition provided that a wrapping density of ∼20% by mass is not exceeded.

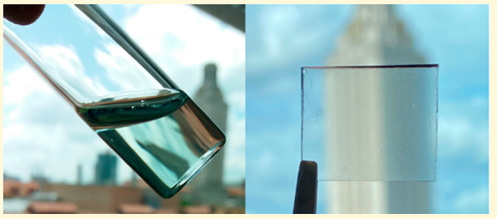

INTRODUCTION

Among transparent conducting oxides, tin-doped indium oxide (ITO) nanocrystals have attracted considerable interest over the past decade as a dynamic electrochromic material for next-generation smart windows.[1−8] Owing to their localized surface plasmon resonance (LSPR) and low carrier concentration (∼10^{20}−10^{21} cm^{-3}), ITO nanocrystals strongly absorb near-infrared (NIR) wavelengths of light between 1500 and 2000 nm. This optical response can be tuned drastically as a function of the nanostructure of the material. Colloidal synthesis methods allow researchers to customize the strength and range of NIR modulation as a function of size, shape, and concentration and distribution of tin dopants,[9−14] while reversible electrochemical doping by subjecting ITO nanocrystals to an external bias achieves greater shifts in absorption intensity and frequency.[1−3,8,15−17] Moreover, since their electrochemical charging is capacitive in nature rather than intercalative, ITO nanocrystals exhibit exceptional NIR electrochromic performance including fast switching kinetics, high coloration efficiency, and extended cycling stability compared to conventional bulk metal oxides.[1−3,5]

Nanocrystal dispersions are suitable for lower cost, high throughput, and more energy efficient solution processing methods for thin films. Additional advantages of wet depositions[3,5,18] that do not rely on high temperatures and ultrahigh vacuum include compatibility with diverse substrates, especially flexible ones, and the fabrication of homogeneous composites with precise compositional control of the different elements. However, the deposition of nanocrystal thin films is typically achieved from nonaqueous, hazardous, and flammable solvents. Specifically, as-synthesized nanocrystals are stabilized by hydrophobic organic ligands and are therefore deposited from nonpolar solvents (e.g., toluene, hexane, octane, etc.).[9,11,19] Because these insulating organic ligands obstruct electronic conductivity across the thin film and intimate contact with the electrolyte in devices, either harsh thermal or chemical postdeposition treatments[1,20] (high temperature annealing and/or soaking in acidic/alkaline solutions), or the removal of ligands in solution before deposition using nitrosonium or Meerwein's salts,[21,22] are needed. The latter yields nanocrystal dispersions in polar solvents such as various formamides, dimethyl sulfoxide, and acetonitrile, but this procedure is not suitable for directly dispersing ITO in aqueous media or mixtures of water and alcohol due to hydroxylation of open-metal sites at the nanocrystal surface, which destabilizes the dispersion. Within this context, there is a clear need to diversify the solvent compatibility of inorganic nanocrystals and develop methods to handle ITO and other metal oxides in water and solvents of low toxicity. This is

Received: June 8, 2020
Revised: September 23, 2020
Published: October 2, 2020

https://dx.doi.org/10.1021/acs.chemmater.0c02399
Chem. Mater. 2020, 32, 8401−8411

particularly relevant to deposition techniques that involve large quantities of vapor effluents such as spray coating,[8,23,24] which is one of the leading candidates for the economically scalable and high throughput fabrication of optical quality nanocrystal thin films.

So far, the primary strategy to disperse nanocrystals in aqueous solvent is to functionalize their surface with hydrophilic molecules. To this end, two approaches have mostly been explored: ligand exchange with inorganic oxoanions and polyoxometalates,[25,26] and with polymers and other organic molecules.[27−35] Stabilizing semiconductor nanocrystals with inorganic ligands grants conductive pathways to the film along with circumventing postdeposition ligand removal and conferring additional properties to the composite. In particular, aqueous dispersions of ITO nanocrystals functionalized with polyoxoniobates enable the direct deposition of homogeneous and tunable NbO_x glass−ITO composites that display selective and dual-band (visible and infrared) electrochromic modulation.[36,37] Nevertheless, this precursor dispersion is strongly alkaline, which is not necessarily suitable for all applications and composite assemblies, and converting the polyoxoniobate matrix into NbO_x requires additional treatment such as high temperature annealing or dipping the composite in an acidic solution. However, while polymer-wrapping metal oxide nanocrystals have been used to achieve aqueous dispersions for various biomedical imaging applications,[35,38−40] this strategy has been less explored for the development of new electrochromic nanomaterials and devices. This is possibly due to challenges related to finding a hydrophilic polymer that adsorbs on the metal oxide surface without restricting electron transport and therefore optoelectronic properties. Notably, Mendelsberg and co-workers[29] demonstrated that ligand-stripped ITO nanocrystals wrapped with the diblock copolymer poly(ethylene oxide)-*b*-poly(*N*,*N*-dimethylacrylamide) (PEO-*b*-PDMA) can be dispersed in water and undergo redox reactions with chemical species in solution. In this case, the PDMA block adsorbs on the bare ITO surface while the PEO block provides steric stabilization. Similarly, poly(acrylic acid)-derived polymers can functionalize bare nanocrystals due to the strong coordination between anionic carboxylate species and metal atoms.[27] In particular, poly(acrylic acid) grafted with methoxy-terminated poly(ethylene oxide) (PAA-$mPEO_4$) has been successfully attached to iron oxide[27] and rare earth metal oxide nanocrystals,[28] but redox reactions with these composites have not been investigated to our knowledge. Beyond their hydrophilic and biocompatible properties, PEO-functionalized ITO nanocrystals could potentially be integrated into electrochromic devices, without the need for additional processing steps to remove the organic layer, since PEO is known to effectively conduct Li^+.[41−44] However, systematic studies on the influence of surface chemistry and polymer adsorption conditions on the morphology and properties of polymer-wrapped metal oxide nanocrystal thin films are needed toward the systematic engineering of these materials. Indeed, previous developments related to other hybrid polymer/metal oxide structures used as electrochromic materials, such as ITO surfaces functionalized with polythiophene,[45] polypyrrole,[46] or polyaniline,[47,48] have shown that the electrochromic response was intrinsically dependent on the polymer processing conditions and resulting composition/thickness.

In this work, we functionalize ITO nanocrystals with PAA-$mPEO_4$ to achieve colloidally stable aqueous "inks" suitable for the spray coating of optical quality electrochromic thin films in a more energy efficient and less toxic way. We expand on the polymer wrapping method developed previously by Duong and co-workers[27] to explore conditions favorable for PAA-$mPEO_4$ adsorption on ITO and to control the wrapping density of the polymer layer by varying the pH and species present in the exchange solution (borate buffer, hydroxides, or pure Milli-Q water). Initially, we identify a pH dependence of the extent of PAA-$mPEO_4$ adsorption and thus colloid stability. Then, we compare the morphology and electrochromic behavior of thin films obtained from ITO with varying PAA-$mPEO_4$ wrapping densities. We find that while maximizing polymer coverage results in the most stable colloidal inks, moderate polymer coverage on the nanocrystal surface (10−22% by mass) leads to optimal electrochromic performance in terms of optical contrast, reversibility, and coloration efficiency that is comparable to the performance of conventional ITO nanocrystal films.

EXPERIMENTAL SECTION

Materials. All chemicals were used as received and without further purification. Indium acetate ($In(ac)_3$, 99.99% trace metal basis), tin(II) acetate ($Sn(ac)_2$), oleylamine (technical grade, 70%), oleic acid (technical grade, 90%), *N*,*N*-dimethylformamide (ACS reagent, ≥ 99.8%), nitrosonium tetrafluoroborate (95%), sodium tetraborate salt, hydrochloric acid, and tetraethylene glycol dimethyl ether (tetraglyme, ≥ 99%) were purchased from Sigma-Aldrich. Hexane (ACS reagent, various methylpentanes 4.2%, ≥ 98.5%), reagent alcohol (ethanol 88−91%, methanol 4.0−5.0%, isopropyl alcohol 4.5−5.5%), and toluene (≥99.5%) were purchased from Fisher Scientific. Lithium bis(trifluoromethanesulfonyl)imide (Li-TFSI, 3 M Fluorad) was purchased from 3M. Fluorine-doped tin oxide (FTO)-coated glass substrates (70 Ω/sq sheet resistance) were purchased from Pilkington (NSG TECTM 70) and silicon substrates were purchased from Virginia Semiconductor Inc.

Nanocrystal Synthesis. Tin-doped indium oxide (ITO) nanocrystals were synthesized using a standard Schlenk line technique and under inert conditions. The synthesis was adapted from previously established colloidal methods.[11,19] Briefly, 2.5 g (8.6 mmol) $In(ac)_3$ and 0.225 g (0.95 mmol) $Sn(ac)_2$ were mixed with 10 mL of oleylamine and degassed under vacuum for 1 h at 120 °C. The solution was then heated to 230 °C under nitrogen and was reacted for 1 h. After cooling to 60 °C, 5 mL of toluene and 1 mL of oleic acid were added to the solution. The ITO nanocrystals were purified and recovered by adding reagent alcohol, centrifuging, and redispersing in toluene. After adding 100 μL of oleic acid to the ITO dispersion in toluene, four more washing cycles were performed (precipitation with reagent alcohol, centrifugation, and redispersion in toluene).

Ligand Stripping Procedure. The hydrophobic ligands bound to the ITO surface were chemically removed using nitrosonium tetrafluoroborate ($NOBF_4$) following a procedure reported previously.[21,26,27,36,49] Briefly, 2 mL of toluene containing ∼45 mg of ITO nanocrystals, originally capped with a mix of oleylamine and oleic acid molecules, were combined with 2 mL of 0.1 M $NOBF_4$ in *N*,*N*-dimethylformamide (DMF). Ligand removal was then promoted by sonication, which led to the transfer of bare ITO nanocrystals from toluene to DMF. The ITO was recovered by precipitating with toluene, centrifuging at 7500 rpm for 5 min, and redispersing in DMF and purified by repeating this washing cycle seven times.

Polymer Wrapping Procedure. PAA-$mPEO_4$ random copolymer was synthesized as described previously.[28] Bare ITO was polymer-wrapped by adapting methods previously developed for other nanocrystal and polymer compositions by Helms, Milliron, and co-workers.[27,29] Briefly, 10 mg of PAA-$mPEO_4$ were dissolved in 700 μL of DMF under gentle stirring. Once the polymer was completely dissolved, 300 μL of 90 mg/mL ligand-stripped ITO in DMF were added dropwise to the polymer solution (final volume 1 mL, 10 mg of

https://dx.doi.org/10.1021/acs.chemmater.0c02399
Chem. Mater. 2020, 32, 8401−8411

Scheme 1. Illustration of the PAA-mPEO$_4$ Wrapping Procedure of ITO Nanocrystals

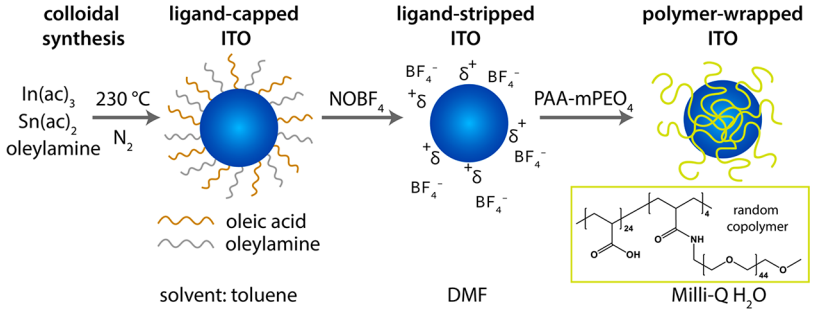

PAA-mPEO$_4$ and 27 mg of ITO). The mixture was stirred at 400 rpm for 24 h and subsequently added dropwise under constant stirring to an aqueous solution (19 mL) of either pure Milli-Q water (pH 6.5) or 50 mM borate buffer (pH 7.9, 8.5, or 9.1), which is henceforth referred to as the exchange solution. After stirring at 600 rpm for 48 h, the exchange solution containing PAA-mPEO$_4$-wrapped ITO was purified with Milli-Q water by spin dialysis using 50 kDa Millipore Amicon Ultra centrifugal tubes. All aqueous dispersions were stable during spin dialysis, except for the one processed from the borate buffer exchange solution at pH 9.1, which precipitated out of solution. In this case, the PAA-mPEO$_4$-wrapped ITO nanocrystal precipitate was resuspended in Milli-Q water by sonicating for 30 min, which resulted in a cloudier solution than the samples processed in the exchange solutions of lower pH. All final dispersions in Milli-Q water were filtered through a 0.45 μm PVDF syringe filter (Acrodisc, Pall).

Polymer-Wrapped ITO Spray Coating. Films of PAA-mPEO$_4$-wrapped ITO nanocrystals were deposited onto 1.5 × 2.0 × 0.4 cm^3 conductive FTO glass or 2.0 × 2.0 cm^2 silicon substrates from ∼8 mg/mL aqueous dispersions using an ExactaCoat (Sono-Tek) spray coater. Deposition was achieved at room temperature using a 0.05 mL/min flow rate, a nozzle-substrate distance of 8.5 cm, a carrier gas (N_2) pressure of 0.90 kPa, and a nozzle moving speed of 8 mm/s following a S-shaped motion with a spacing of 4 mm between each arc. This raster pattern was applied 10 consecutive times, resulting in coatings with an average thickness of ∼130 nm (values are determined on a Vecco Dektak 150+ Profiler instrument). Samples were finally dried on a hot plate at 120 °C for 10 min to drive water evaporation.

Electron Microscopy. Transmission Electron Microscopy (TEM) micrographs of the PAA-mPEO$_4$-wrapped ITO dispersions were captured by a JEOL 2010F instrument with a Schottky Field Emission source operated at 200 kV. Samples were prepared by dropcasting the aqueous dispersions on TEM grids (Pelco ultrathin carbon-A 400 mesh grid, Ted Pella), allowing them to fully evaporate under ambient conditions, and subsequently wicking them with acetonitrile to mitigate the degradation of hydrocarbons during exposure to the electron beam. Scanning electron microscopy (SEM) images of the resulting PAA-mPEO$_4$-wrapped ITO thin films sprayed onto silicon were captured on a Hitachi S5500 instrument at a 15 kV accelerating voltage.

Fourier Transform Infrared Spectroscopy (FTIR). FTIR spectra of polymer-wrapped ITO films sprayed onto undoped, double side polished silicon were recorded in transmission geometry with a Bruker Vertex 70 spectrometer. Peak intensities from PAA-mPEO$_4$ vibrational modes reflect the relative polymer content across samples since dispersions of equivalent ITO concentration were spray coated to obtain films of similar ITO volume fraction.

Dynamic Light Scattering and Zeta Potential. Hydrodynamic diameter and zeta potential measurements were conducted on a Malvern Zetasizer Nano ZS. ITO nanocrystal dispersions were enclosed in disposable plastic micro cuvettes (ZEN0040, Malvern) for size measurements and in a glass cuvette to record zeta potentials with a dip cell (ZEN 1002, Malvern).

Thermogravimetric Analysis (TGA). The amount of PAA-mPEO$_4$ coating the nanocrystal surface was determined by TGA (Mettler Toledo TGA 2). In a typical experiment, 100 μL of polymer-wrapped ITO dispersion were added to a disposable aluminum crucible and the water was evaporated under vacuum at room temperature over 24 h. Samples were run in air from 30 to 600 °C at a 5 °C/min ramp rate.

Electrochemical Modulation. A custom-built spectroelectrochemical cell connected to a potentiostat (Biologic VMP3) and spectrometer (ASD Quality Spec Pro) was used for electrochemical and in situ optical measurements in an Ar glovebox. The electrochromic performance of the spray coated ITO films was measured in a three-electrode and half-cell configuration, in which the ITO film deposited on FTO-coated glass (working electrode) and Li foil (both counter and reference electrode) are immersed in an electrolyte (1.0 M LiTFSI in tetraglyme). Optical modulation was induced by switching the applied potential between +4.0 (transparent state) and +1.5 V vs Li/Li$^+$ (dark state). Each potential was held for 1 min. To measure coloration efficiency, samples were first fully bleached by applying a + 4.0 V potential bias for 10 min, then subjected to galvanostatic coulometry at −15 μA (corresponding to 10 times the value of the leakage current) during which consecutive absorbance spectra were recorded at a specific time interval of 5 s until the electrode reached a + 1.5 V potential value corresponding to a fully darkened state.

RESULTS AND DISCUSSION

ITO (∼10 at% Sn) nanocrystals were obtained from a heat-up colloidal synthesis and the decomposition of In and Sn acetate precursors by aminolysis (cf., Experimental Section). The as-synthesized nanocrystals were stabilized with hydrophobic ligands (a mixture of oleylamine and oleic acid molecules) and dispersed in a nonpolar solvent (toluene). Then, the ITO nanocrystals were transferred into aqueous media after performing a two-step ligand exchange procedure: ligand removal with NOBF$_4$ to produce stable ITO dispersions in DMF followed by polymer wrapping with PAA-mPEO$_4$ in water (Scheme 1).

Polymer wrapping was performed in aqueous solutions of varying pH (Milli-Q water at pH 6.5 and borate buffers at pH 7.9, 8.5, and 9.1) to explore conditions favorable for both the colloidal stability of ITO and the electrochromic modulation when further processed into thin films. To produce the final colloid (Figure 1, insets), each exchange solution containing PAA-mPEO$_4$-wrapped ITO was purified via spin-dialysis with Milli-Q water. Characterization of the ITO morphology after each surface modification step confirmed that our ligand exchange procedure is not destructive. TEM images of the final dispersions (Figure 1) show that, in all four cases, the original morphology (Figure S1 of the Supporting Information, SI) of the ITO is conserved without signs of etching. The only noticeable difference between these TEMs is the presence of aggregates in the dispersion obtained from the exchange

https://dx.doi.org/10.1021/acs.chemmater.0c02399
Chem. Mater. 2020, 32, 8401−8411

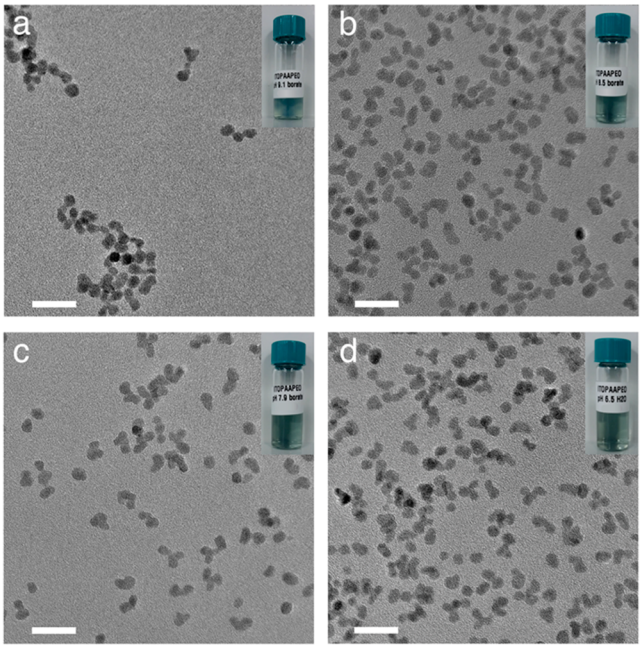

Figure 1. Transmission electron microscopy of ITO aqueous dispersions after PAA-mPEO$_4$ wrapping in: (a) pH 9.1 borate buffer, (b) pH 8.5 borate buffer, (c) pH 7.9 borate buffer, and (d) pH 6.5 Milli-Q water. Scale bars = 20 nm. Insets: photographs of the corresponding vial.

solution at pH 9.1 (Figure 1a), likely due to poor PAA-mPEO$_4$ coverage.

To investigate the influence of pH on the colloidal stability of PAA-mPEO$_4$-wrapped ITO, we measured the hydrodynamic diameter and zeta potential of the four final dispersions described above. As shown in Figure 2a, transferring PAA-mPEO$_4$-wrapped ITO into pure Milli-Q water and mildly alkaline borate buffers (pH 7.9 and 8.5) yields a hydrodynamic diameter of ∼12 nm while raising the pH to 9.1 leads to a larger hydrodynamic diameter (∼25 nm) with a broader distribution. Considering that the hydrodynamic diameter of both ligand-capped and ligand-stripped ITO nanocrystals is ∼10 nm (Figure S2), we determined that aqueous exchange solutions at pH 6.5, 7.9, and 8.5 stabilize discrete ITO nanocrystals (hydrodynamic diameter of ∼12 nm), whereas the exchange solution at pH 9.1 favors the formation of ITO aggregates (hydrodynamic diameter of ∼25 nm). Likewise, the magnitude of the zeta potential of the dispersion obtained from the exchange solution at pH 9.1 is lower than 20 mV and thus indicative of poor colloidal stability, unlike the magnitude of the other three dispersions (Figure 2b). In addition, a negative zeta potential value for all four PAA-mPEO$_4$-wrapped ITO dispersions is consistent with the coordination of anionic carboxylate groups from the PAA backbone to the ITO nanocrystal surface. However, considering that the samples obtained from the buffer exchange solutions were simultaneously exposed to carboxylate and borate anions, further characterization is needed to identify the species adsorbed on the surface.

To confirm the adsorption of PAA-mPEO$_4$ on the ITO surface and identify the exchange solution conditions that facilitate this interaction, we tracked and quantified polymer adsorption by FTIR and TGA. We detect characteristic FTIR bands from PAA-mPEO$_4$ in all samples and find that as the pH of the exchange solution increases, the amount of PAA-mPEO$_4$ wrapping decreases. Examining the 2400−4000 cm^{-1} spectral region reveals a gradual decrease in the intensity of C−H stretches (2900 cm^{-1}) from both PAA and PEO moieties[50,51] as pH increases (Figure 3a). In the 1400−1750 cm^{-1} spectral region, we observe the bands characteristic of asymmetric and symmetric −COO$^-$ stretches at 1574 and 1452 cm^{-1} (Figure 3b),[52,53] respectively, instead of the strong peak from −C═O stretches present in the FTIR spectrum of as-synthesized PAA-mPEO$_4$ (Figure S3). The absence of carbonyl stretches in the spectra of the polymer-wrapped ITO nanocrystal dispersions suggests that PAA adsorption is driven by the coordination between anionic carboxylates and exposed metal atoms on the nanocrystal surface. In fact, the asymmetric and symmetric carboxylate stretches are separated by $\Delta\nu$ = 122 cm^{-1}, which is close to the $\Delta\nu$ values reported for indium-carboxylate[54,55] and iron-carboxylate[53] bidentate ligand coordination. Moreover, as pH increases, we note the gradual weakening of C−O−C stretches from PEO[50] (1140 cm^{-1}) accompanied by the emergence of borate bands such as B−OH stretches from tetrahedral B(OH)$_4^-$ around 1030 cm^{-1} and B−O stretches from trigonal (BOH)$_3$ around 1412−1354 cm^{-1} (see Figure S3 for a borate reference spectrum).[56−58] These borate peaks are particularly predominant in the spectrum of the ITO dispersion processed from the exchange solution at pH 9.1. In addition, low PAA-mPEO$_4$ adsorption could favor the formation of In−OH and Sn−OH on the nanocrystal surface,

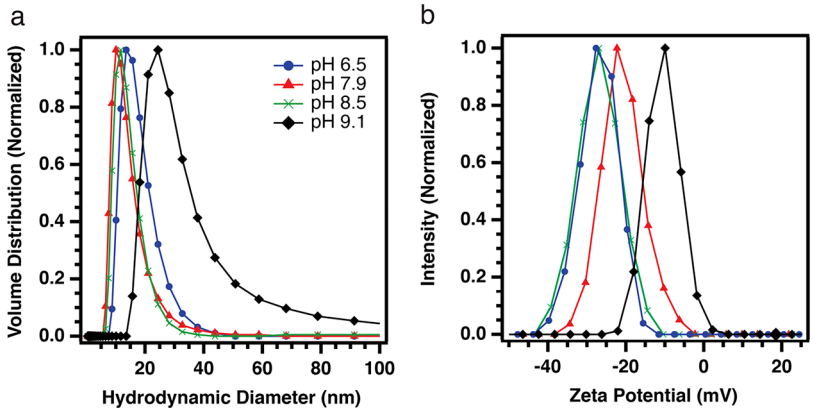

Figure 2. Colloidal stability of ITO aqueous dispersions after PAA-mPEO$_4$ wrapping in exchange solutions of different pH: (a) hydrodynamic diameter comparison and (b) zeta potential comparison.

https://dx.doi.org/10.1021/acs.chemmater.0c02399
Chem. Mater. 2020, 32, 8401−8411

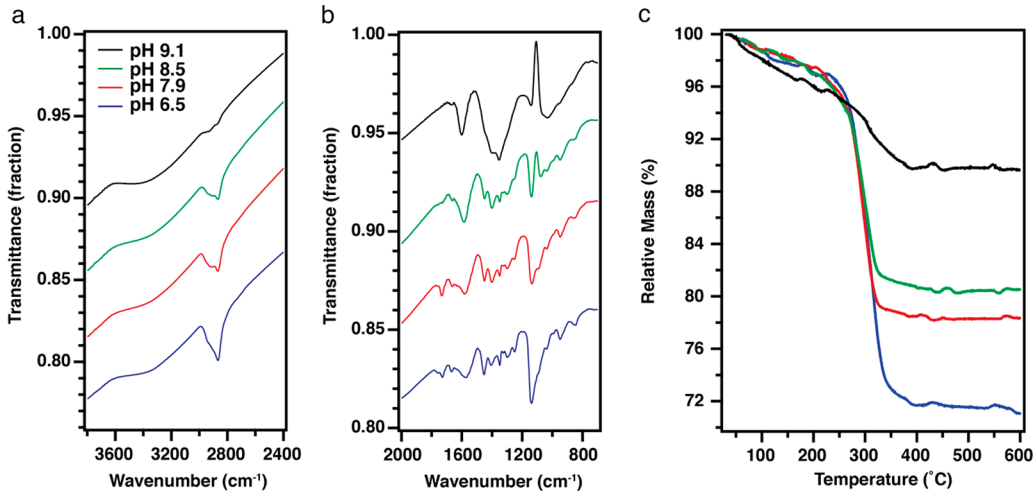

Figure 3. PAA-mPEO$_4$ adsorption on ITO is influenced by the pH of the exchange solution: (a) FTIR spectra showing a decrease in C−H stretch intensity with increasing pH—the sloping profile in the spectra is caused by absorption due to localized surface plasmon resonance, (b) FTIR spectra showing a decrease in C−O−C stretch intensity and the emergence of borate vibrational modes with increasing pH, and (c) TGA confirming a decrease in mass loss due to PAA-mPEO$_4$ decomposition with increasing pH. FTIR spectra were arbitrarily offset for clarity. Relative peak intensities are representative of PAA-mPEO$_4$ content since samples were prepared from dispersions having the same ITO concentration and resulted in films of similar thickness.

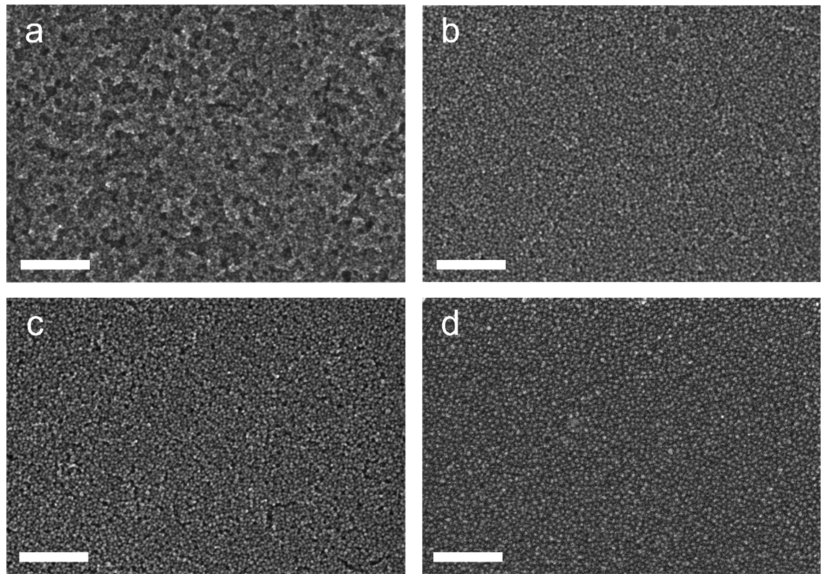

Figure 4. Scanning electron microscopy of ITO nanocrystal films spray coated onto silicon substrates from aqueous dispersion after PAA-mPEO$_4$ wrapping in: (a) pH 9.1 borate buffer (10% polymer by mass), (b) pH 8.5 borate buffer (18% polymer by mass), (c) pH 7.9 borate buffer (22% polymer by mass), and (d) pH 6.5 Milli-Q water (28% polymer by mass). Scale bar= 100 nm.

which could explain the broadness of the peak assigned to B−OH stretches since In−OH and Sn−OH bending modes[59] appear around 1100 cm^{-1}. On the basis of these FTIR results, we infer that borate anions compete with PAA-mPEO$_4$ for adsorption sites on the ITO surface and significantly prevent polymer adsorption when the buffer pH is around 9.1. Since the pK_a of boric acid is close to 9.1,[60] we hypothesized that the concentration of borate anions at pH < 9.1 would decrease, thus improving the likelihood of PAA-mPEO$_4$ adsorption relative to borate. Although borate adsorption is favored at pH > 9.1, it is important to note that borate alone does not provide sufficient electrostatic stabilization since ITO dispersions prepared in the absence of polymer exhibit significant aggregation and precipitate out of solution in a matter of hours (Figure S4). Therefore, the extent of electrostatic plus steric repulsion that PAA-mPEO$_4$ wrapping provides is key to ensure the colloidal stability of ITO aqueous dispersions over extended periods of time, even months. Quantifying polymer wrapping in these four dispersions by TGA further supports our conclusions, since the mass loss associated with the thermal decomposition of PAA-mPEO$_4$ decreases as pH increases: 28% mass loss for pH 6.5, 22% mass loss for pH 7.9, 18% mass loss for pH 8.5, and 10% mass loss for pH 9.1 (Figure 3c).

To deconvolute the influence of pH from the presence of borate anions on PAA-mPEO$_4$ adsorption, we used alternative exchange solutions containing potassium hydroxide at different pH (8.3 and 12.4). The exchange solution at pH 8.3 produces an ITO dispersion with a PAA-mPEO$_4$ wrapping density comparable to the wrapping density of the dispersion

https://dx.doi.org/10.1021/acs.chemmater.0c02399
Chem. Mater. 2020, 32, 8401−8411

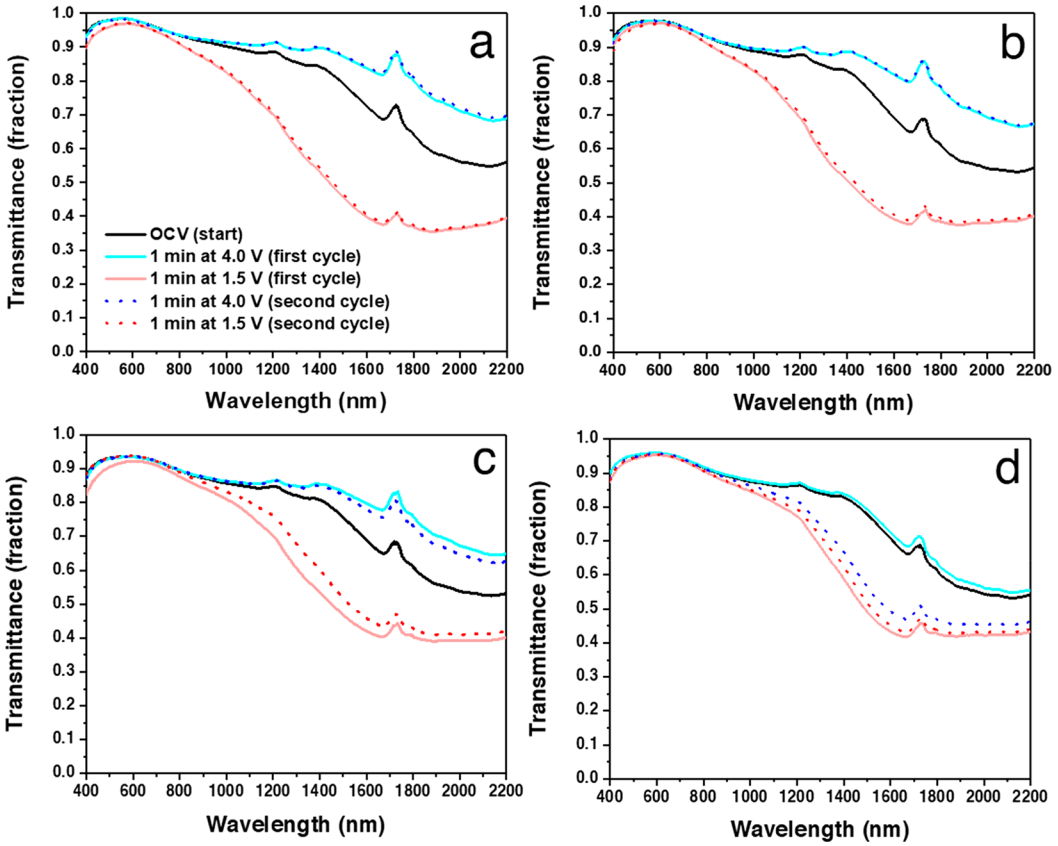

Figure 5. Electrochromic modulation of ITO films spray coated onto FTO glass from ITO aqueous dispersion after PAA-mPEO$_4$ wrapping in: (a) pH 9.1 borate buffer (10% polymer by mass), (b) pH 8.5 borate buffer (18% polymer by mass), (c) pH 7.9 borate buffer (22% polymer by mass), and (d) pH 6.5 Milli-Q water (28% polymer by mass). Transmittance spectra were recorded after applying 4.0 V ("bleached" state, blue curves) and 1.5 V ("darkened" state, red curves), referenced to a Li/Li$^+$ electrode in 1.0 M LiTFSI in tetraglyme, from the initial as-deposited state (black curves) at open circuit voltage. Solid lines correspond to the first potentiostatic "darkened-bleached" modulation cycle, and dotted lines correspond to the second cycle.

processed in Milli-Q water at pH 6.5 (30% mass loss by TGA, Figure S5), rather than the one obtained for pH 8.5 with borate (18% mass loss by TGA). The FTIR spectra of the samples obtained from aqueous solutions with pH 6.5 and 8.3 are also in agreement with the TGA analysis (Figure S5). It is important to note that PAA-mPEO$_4$ wrapping of ITO in a phosphate buffer exchange solution at pH 6.5 led to the irreversible aggregation of ITO and precipitation, which is why we were not able to control for the presence of additional anions at this pH. Nonetheless, the exchange solution at pH 12.4 resulted in an ITO dispersion with a PAA-mPEO$_4$ wrapping density (8% mass loss by TGA) comparable to the pH 9.1 borate buffer case with FTIR bands characteristic of indium-hydroxyl coordination at 1100 cm^{-1} and O−H around 1630−1620 cm^{-1} instead of PAA-mPEO$_4$.[59] Therefore, as observed with borate buffer exchange solutions, hydroxide anions in solution compete with PAA-mPEO$_4$ for coordination sites on the ITO surface and significantly inhibit polymer adsorption above a threshold pH. The ability to tune PAA-mPEO$_4$ absorption on the ITO surface is thus not unique to borate anions; however, using borate buffer instead of highly alkaline hydroxide exchange solutions is preferred to avoid etching the ITO.

PAA-mPEO$_4$-wrapped ITO dispersions (∼8 mg/mL) were used as aqueous "inks" to produce uniform films with an average thickness of ∼130 nm on 1.5 × 2.0 cm^2 substrates through ultrasonic spray deposition under ambient conditions (room temperature and atmospheric pressure). Films were processed by applying a specific spray pattern at nozzle-substrate distance of 8.5 cm (cf., Experimental Section). SEM top-view images of ITO films show a complete coverage of the substrates (Figure 4). Film morphology is directly affected by the extent of polymer wrapping: using an aggregated colloid (10% PAA-mPEO$_4$ by mass) as the sprayed "ink" produces rough layers with obvious porosity (Figure 4a) while stable dispersions of discrete ITO nanocrystals with greater polymer wrapping (18−28% PAA-mPEO$_4$ by mass) lead to smooth and uniform optical quality films (Figure 4b−d). Atomic force microscopy measurements confirm the decrease of mean roughness R_a values for colloidally stable precursor inks (Table S1).

The electrochromic behavior of ITO films, with varying PAA-mPEO$_4$ wrapping densities, spray coated onto FTO glass was investigated. Spectroelectrochemical measurements (Figure 5) were conducted in a half cell configuration with the PAA-mPEO$_4$−ITO film (working electrode) and lithium foil (counter and reference electrodes) immersed in 1.0 M LiTFSI in tetraglyme electrolyte solution. First, the ITO films are bleached from their open circuit voltage state (black curve) to a fully transparent state (solid blue curve) by applying +4.0 V vs Li/Li$^+$ and then darkened in the near-infrared (NIR) by charging at +1.5 V (solid red curve). As established in previous studies,[1−3] such modulation of optical absorption results from the reversible shift of the LSPR peak energy and intensity. This

https://dx.doi.org/10.1021/acs.chemmater.0c02399
Chem. Mater. 2020, 32, 8401−8411

shift is induced by the capacitive charging of the ITO nanocrystals in response to the externally applied electrochemical potential, modifying the concentration and spatial distribution of the free electrons in the nanocrystals. This capacitive mechanism has been shown to specifically enable rapid and efficient NIR-selective modulation abilities as well as long cycling durability in such electrochromic layers of ITO as well as other doped metal oxides such as antimony-doped tin oxide ATO[61] or aluminum-doped zinc oxide AZO.[2]

We observe that the amplitude of NIR modulation, measured at λ = 1900 nm, for the first electrochemical charging/discharging cycle (solid lines in Figure 5) is inversely correlated to the PAA-mPEO$_4$ content in the composite films. Optical contrast decreases as the amount polymer adsorbed on the nanocrystal surface increases, with the conditions favoring the highest PAA-mPEO$_4$ coverage giving rise to the smallest dynamic optical range. Specifically, the composite films achieve 39% (ΔT = 75−36, Figure 5a), 34% (ΔT = 72−38, Figure 5b), 31% (ΔT = 70−39, Figure 5c), and only 17% (ΔT = 59−42, Figure 5d) NIR modulation, for 10, 18, 22, and 28% polymer wrapping by mass, respectively. After the second potentiostatic cycle, the effect of polymer wrapping density on optical modulation becomes more significant (dotted lines in Figure 5). While the film with the highest PAA-mPEO$_4$ wrapping density cannot be bleached back to its initial fully transparent state (2% contrast or ΔT = 45−43, Figure 5d), ITO films with lower wrapping density exhibit large and stable contrasts (39% or ΔT = 75−36 in Figure 5a, 33% or ΔT = 72−39 in Figure 5b, and 27% or ΔT = 68−41 in Figure 5c). These results suggest that exceeding a PAA-mPEO$_4$ wrapping density threshold (of at least 28% by relative mass) hinders the electrochromic reversibility of the composite film. To distinguish between the impact of PAA-mPEO$_4$ adsorption and the persistence of borate anions on the optical modulation, we recorded the spectroelectrochemical behavior of films deposited from PAA-mPEO$_4$-wrapped ITO processed in potassium hydroxide exchange solutions (Figure S6). Films of ITO dispersions processed in the absence of borate with a wrapping density of 30% relative mass exhibit limited and irreversible optical contrast (10% or ΔT = 55−45). Conversely, films of ITO dispersions processed in the absence of borate with a wrapping density of 8% relative mass achieve large and stable optical contrast (43% or ΔT = 73−30). Hence, the polymer itself, when present at a high wrapping density, is responsible for poor electrochromic modulation.

Coloration efficiency (CE), a measure of the change in optical density ΔOD per inserted charge density ΔQ, was established by fitting the linear region of the corresponding ΔOD vs ΔQ curves obtained from galvanostatic measurements (Figure 6). PAA-mPEO$_4$ wrapping on the ITO surface does not qualitatively diminish the electrochromic performance expected for capacitive charging of plasmonic metal oxides nanocrystals.[3,5,62] The four films deposited from ITO dispersions exposed to Milli-Q water and borate buffers exhibit CE values of similar order of magnitude as the values previously reported for bare ITO nanocrystal films: 535, 587, 673, and 802 cm^2/C in order of decreasing PAA-mPEO$_4$ wrapping density (or increasing exchange solution pH).[1,63,64] Furthermore, tracking the evolution of ΔOD over time (Figure S7) shows that reaching a PAA-mPEO$_4$ wrapping density of 28% relative mass leads to slower rate of coloration (ΔOD = 0.14 is reached after 600 s) relative to the other three films (ΔOD = 0.24, 0.28, and 0.32, in order of decreasing polymer wrapping density, is reached after 300 s) for the same amount of inserted charge (~1.4 mC/cm^2). Thus, high extents of PAA-mPEO$_4$ wrapping on ITO seem to limit the kinetics of coloration in the composite films.

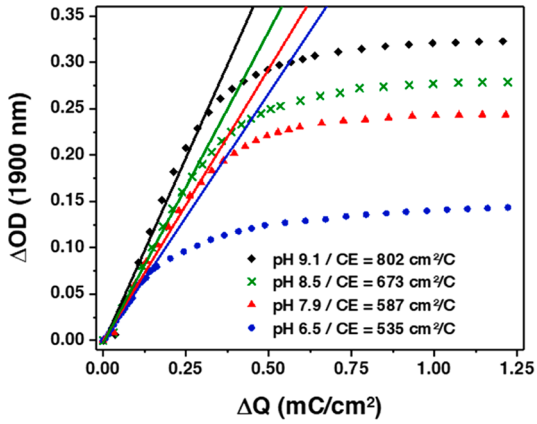

Figure 6. Coloration efficiency (CE) analysis of thin films spray coated onto conductive glass substrates from PAA-mPEO$_4$-wrapped ITO nanocrystals dispersions processed at different pH and buffer conditions.

In view of the results summarized in Table 1, considering the extent of PAA-mPEO$_4$ wrapping on the ITO surface is crucial to optimize electrochromic performance. In this system, ITO dispersions with moderate PAA-mPEO$_4$ wrapping (10−22% polymer by mass) demonstrate excellent electrochromic performance in terms of optical modulation, coloration efficiency, and charging/discharging kinetics. However, ITO nanocrystals with minimal PAA-mPEO$_4$ wrapping (i.e., 10% PAA-mPEO$_4$ by mass) are not necessarily advantageous "inks" for the solution deposition of thin films because this colloid is not stable during the ligand exchange process, needs to be resuspended using sonication, and begins showing visible signs of precipitation after a few days, which suggests the formation of uncontrolled aggregates over time and could potentially affect batch-to-batch reproducibility. Despite the fact that PAA- and PEO-based polymers are widely used as solid electrolytes to enhance Li$^+$ transport,[41,44] we also suspect that excessive wrapping with electronically insulating PAA-mPEO$_4$ could result in poor contact between neighboring ITO nanocrystals in the film and severely restrict electron conduction. The poor conductivity is supported by additional cyclic voltammetry measurements (Figure S8) showing that the ITO film with the highest PAA-mPEO$_4$ wrapping density (28% by mass) exhibits a notably lower current density than the other three cases (10, 18, and 22% by mass). Although beyond the scope of this work, further investigations would help elucidate the charge transport limitations of incorporating PAA-mPEO$_4$ into plasmonic nanocrystal films for electrochromic windows and other electrochemical devices. We envision that such studies could even motivate the design and implementation of other copolymers to circumvent the current disadvantages of our system.

CONCLUSIONS

We developed a method to produce colloidally stable dispersions of PAA-mPEO$_4$-wrapped ITO nanocrystals in water and demonstrated an environmentally conscious ("green") processing alternative for electrochromic thin films via ultrasonic spray deposition. We investigated the influence

https://dx.doi.org/10.1021/acs.chemmater.0c02399
Chem. Mater. 2020, 32, 8401−8411

Table 1. Influence of PAA-mPEO$_4$ wrapping conditions on colloidal stability of ITO in water and electrochromic modulation of composite films[a]

			ΔT (%)			
exchange solution	Zeta potential (mV)	polymer wrapping by mass (%)	1st cycle	2nd cycle	CE (cm^2/C)	reversible electrochromism?
pH 9.1 (borate)	−10	10	39	39	802	yes
pH 8.5 (borate)	−27	18	34	33	673	yes
pH 7.9 (borate)	−22	22	31	27	587	yes
pH 6.5 (Milli-Q)	−28	28	17	2	535	no

[a]Optical contrast and CE are measured at λ= 1900 nm.

of the exchange solution conditions (pH and anionic species) on the extent of PAA-mPEO$_4$ wrapping on the ITO surface, which directly impacts the colloidal stability in water and thereby the morphology of the sprayed films. Although the as-deposited thin films modulate NIR light without the need to remove the polymer through postdeposition thermal or chemical treatments, we found that exceeding a polymer-wrapping density threshold results in irreversibly darkened films. Despite this limitation, we demonstrated the utility of ITO nanocrystals moderately wrapped with PAA-mPEO$_4$ as electrochromic films of comparable performance to conventional ligand-free plasmonic ITO films, while also obviating the use of hazardous solvents thus showcasing the utility of our strategy.[1,2,8,63] More specifically, achieving a polymer wrapping density greater than 10% by mass ensures the stability of the colloid at each processing step and circumvents issues related to uncontrolled aggregation over time such as the need for additional sonication before spray deposition and potential batch-to-batch variability, without significantly sacrificing the electrochromic performance of the thin film as long as the polymer wrapping density does not exceed ∼20% by mass.

More generally, we have shown that the interaction between the polymer and the ligand exchange environment (e.g., pH and additional species in the aqueous solution) affects the extent of polymer wrapping and therefore colloidal stability. Control over these parameters allows the reliable deposition of optical quality films and optimization of the properties in composites. Beyond thin film deposition, designing and identifying processing conditions that promote colloidal stability are crucial to achieve multiscale assemblies (e.g., superlattices, gels, micelle-like structures, etc.) of polymer-wrapped nanocrystals with controllable structures and unique properties. Furthermore, we envision that our functionalization method with PAA-mPEO$_4$ could broaden the applicability of ITO nanocrystals to areas where plasmonic metal oxides are less employed and explored such as hydrogels,[64−66] bioassays,[67,68] therapeutics,[69] toxicology studies,[70−73] and other biological applications.

■ ASSOCIATED CONTENT

Supporting Information

The Supporting Information is available free of charge at https://pubs.acs.org/doi/10.1021/acs.chemmater.0c02399.

Details of additional ITO nanocrystal characterization and PAA-mPEO$_4$-wrapped ITO nanocrystal dispersions from potassium hydroxide exchange solutions (TEM, DLS, UV−vis−NIR, FTIR, TGA), film thickness and roughness measurements, and spectroelectrochemistry (PDF)

■ AUTHOR INFORMATION

Corresponding Author

Delia J. Milliron − *McKetta Department of Chemical Engineering, The University of Texas at Austin, Austin, Texas 78712, United States;* orcid.org/0000-0002-8737-451X; Email: milliron@che.utexas.edu

Authors

Anthony Maho − *McKetta Department of Chemical Engineering, The University of Texas at Austin, Austin, Texas 78712, United States; Group of Research in Energy and Environment from Materials (GREENMAT), University of Liège, 4000 Liège, Belgium; Fonds National de la Recherche Scientifique (FRS-FNRS), 1000 Brussels, Belgium;* orcid.org/0000-0002-3813-6240

Camila A. Saez Cabezas − *McKetta Department of Chemical Engineering, The University of Texas at Austin, Austin, Texas 78712, United States;* orcid.org/0000-0002-8734-0096

Kendall A. Meyertons − *McKetta Department of Chemical Engineering, The University of Texas at Austin, Austin, Texas 78712, United States*

Lauren C. Reimnitz − *McKetta Department of Chemical Engineering, The University of Texas at Austin, Austin, Texas 78712, United States;* orcid.org/0000-0003-4570-7176

Swagat Sahu − *The Molecular Foundry, Lawrence Berkeley National Laboratory, Berkeley, California 94720, United States*

Brett A. Helms − *The Molecular Foundry, Lawrence Berkeley National Laboratory, Berkeley, California 94720, United States;* orcid.org/0000-0003-3925-4174

Complete contact information is available at: https://pubs.acs.org/10.1021/acs.chemmater.0c02399

Author Contributions

[#]A.M. and C.A.S.C contributed equally to this work.

Notes

The authors declare the following competing financial interest(s): D.J. Milliron has a financial interest in Heliotrope Technologies, a company pursuing commercialization of electrochromic devices.

■ ACKNOWLEDGMENTS

A.M. is grateful to University of Liège—GREENMAT (Prof. Rudi Cloots, Dr. Catherine Henrist, Dr. Pierre Colson) for scientific guidance as well as administrative and logistic support, and to FRS-FNRS and Wallonie-Bruxelles International (WBI) for postdoctoral fellowship (FC 86864) and mobility funding. This research was partially supported by the National Science Foundation through the Center for Dynamics and Control of Materials: an NSF MRSEC under Cooperative Agreement No. DMR-1720595 and by the Welch Foundation (F-1848). Work at the Molecular Foundry—including polymer

synthesis and characterization—was supported by the Office of Science, Office of Basic Energy Sciences, of the U.S. Department of Energy under Contract No. DE-AC02-05CH11231.

REFERENCES

(1) Garcia, G.; Buonsanti, R.; Runnerstrom, E. L.; Mendelsberg, R. J.; Llordés, A.; Anders, A.; Richardson, T. J.; Milliron, D. J. Dynamically Modulating the Surface Plasmon Resonance of Doped Semiconductor Nanocrystals. *Nano Lett.* **2011**, *11*, 4415−4420.
(2) Garcia, G.; Buonsanti, R.; Llordés, A.; Runnerstrom, E. L.; Bergerud, A.; Milliron, D. J. Near-Infrared Spectrally Selective Plasmonic Electrochromic Thin Films. *Adv. Opt. Mater.* **2013**, *1*, 215−220.
(3) Runnerstrom, E. L.; Llordés, A.; Lounis, S. D.; Milliron, D. J. Nanostructured Electrochromic Smart Windows: Traditional Materials and NIR-Selective Plasmonic Nanocrystals. *Chem. Commun.* **2014**, *50*, 10555−10572.
(4) Granqvist, C. G. Electrochromics for Smart Windows: Oxide-Based Thin Films and Devices. *Thin Solid Films* **2014**, *564*, 1−38.
(5) Wang, Y.; Runnerstrom, E. L.; Milliron, D. J. Switchable Materials for Smart Windows. *Annu. Rev. Chem. Biomol. Eng.* **2016**, *7*, 283−304.
(6) Kriegel, I.; Scotognella, F.; Manna, L. Plasmonic Doped Semiconductor Nanocrystals: Properties, Fabrication, Applications and Perspectives. *Phys. Rep.* **2017**, *674*, 1−52.
(7) Wang, Z.; Wang, X.; Cong, S.; Geng, F.; Zhao, Z. Fusing Electrochromic Technology with Other Advanced Technologies: a New Roadmap for Future Development. *Mater. Sci. Eng., R* **2020**, *140*, 100524.
(8) Maho, A.; Lamela, L. C.; Henrist, C.; Henrard, L.; Tizei, L. H. G.; Kociak, M.; Stéphan, O.; Heo, S.; Milliron, D. J.; Vertruyen, B. Solvothermally-Synthesized Tin-Doped Indium Oxide Plasmonic Nanocrystals Spray-Deposited Onto Glass as Near-Infrared Electrochromic Films. *Sol. Energy Mater. Sol. Cells* **2019**, *200* (1−9), 110014.
(9) Jansons, A. W.; Hutchison, J. E. Continuous Growth of Metal Oxide Nanocrystals: Enhanced Control of Nanocrystal Size and Radial Dopant Distribution. *ACS Nano* **2016**, *10*, 6942−6951.
(10) Crockett, B. M.; Jansons, A. W.; Koskela, K. M.; Johnson, D. W.; Hutchison, J. E. Radial Dopant Placement for Tuning Plasmonic Properties in Metal Oxide Nanocrystals. *ACS Nano* **2017**, *11*, 7719−7728.
(11) Kanehara, M.; Koike, H.; Yoshinaga, T.; Teranishi, T. Indium Tin Oxide Nanoparticles with Compositionally Tunable Surface Plasmon Resonance Frequencies in the Near-IR Region. *J. Am. Chem. Soc.* **2009**, *131*, 17736−17737.
(12) Agrawal, A.; Cho, S. H.; Zandi, O.; Ghosh, S.; Johns, R. W.; Milliron, D. J. Localized Surface Plasmon Resonance in Semiconductor Nanocrystals. *Chem. Rev.* **2018**, *118*, 3121−3207.
(13) Staller, C. M.; Gibbs, S. L.; Saez Cabezas, C. A.; Milliron, D. J. Quantitative Analysis of Extinction Coefficients of Tin-Doped Indium Oxide Nanocrystal Ensembles. *Nano Lett.* **2019**, *19*, 8149−8154.
(14) Cho, S. H.; Roccapriore, K. M.; Dass, C. K.; Ghosh, S.; Choi, J.; Noh, J.; Reimnitz, L. C.; Heo, S.; Kim, K.; Xie, K.; et al. Spectrally Tunable Infrared Plasmonic F,Sn:In_2O_3 Nanocrystal Cubes. *J. Chem. Phys.* **2020**, *152*, 014709.
(15) Agrawal, A.; Kriegel, I.; Runnerstrom, E. L.; Scotognella, F.; Llordés, A.; Milliron, D. J. Rationalizing the Impact of Surface Depletion on Electrochemical Modulation of Plasmon Resonance Absorption in Metal Oxide Nanocrystals. *ACS Photonics* **2018**, *5*, 2044−2050.
(16) Gibbs, S. L.; Staller, C. M.; Milliron, D. J. Surface Depletion Layers in Plasmonic Metal Oxide Nanocrystals. *Acc. Chem. Res.* **2019**, *52*, 2516−2524.
(17) Zandi, O.; Agrawal, A.; Shearer, A. B.; Reimnitz, L. C.; Dahlman, C. J.; Staller, C. M.; Milliron, D. J. Impacts of Surface Depletion on the Plasmonic Properties of Doped Semiconductor Nanocrystals. *Nat. Mater.* **2018**, *17*, 710−717.
(18) Li, X.; Perera, K.; He, J.; Gumyusenge, A.; Mei, J. Solution-Processable Electrochromic Materials and Devices: Roadblocks and Strategies Towards Large-Scale Applications. *J. Mater. Chem. C* **2019**, *7*, 12761−12789.
(19) Choi, S.-I.; Nam, K. M.; Park, B. K.; Seo, W. S.; Park, J. T. Preparation and Optical Properties of Colloidal, Monodisperse, and Highly Crystalline ITO Nanoparticles. *Chem. Mater.* **2008**, *20*, 2609−2611.
(20) Wang, Y.; Kim, J.; Gao, Z.; Zandi, O.; Heo, S.; Banerjee, P.; Milliron, D. J. Disentangling Photochromism and Electrochromism by Blocking Hole Transfer at the Electrolyte Interface. *Chem. Mater.* **2016**, *28*, 7198−7202.
(21) Dong, A.; Ye, X.; Chen, J.; Kang, Y.; Gordon, T.; Kikkawa, J. M.; Murray, C. B. A Generalized Ligand-Exchange Strategy Enabling Sequential Surface Functionalization of Colloidal Nanocrystals. *J. Am. Chem. Soc.* **2011**, *133*, 998−1006.
(22) Rosen, E. L.; Buonsanti, R.; Llordés, A.; Sawvel, A. M.; Milliron, D. J.; Helms, B. A. Exceptionally Mild Reactive Stripping of Native Ligands From Nanocrystal Surfaces by Using Meerwein's Salt. *Angew. Chem., Int. Ed.* **2012**, *51*, 684−689.
(23) Gaspera; Della, E.; Bersani, M.; Cittadini, M.; Guglielmi, M.; Pagani, D.; Noriega, R.; Mehra, S.; Salleo, A.; Martucci, A. Low-Temperature Processed Ga-Doped ZnO Coatings From Colloidal Inks. *J. Am. Chem. Soc.* **2013**, *135*, 3439−3448.
(24) Kumar, N.; Lee, H. B.; Hwang, S.; Kim, T.-W.; Kang, J.-W. Fabrication of Plasmonic Gold-Nanoparticle-Transition Metal Oxides Thin Films for Optoelectronic Applications. *J. Alloys Compd.* **2019**, *775*, 39−50.
(25) Huang, J.; Liu, W.; Dolzhnikov, D. S.; Protesescu, L.; Kovalenko, M. V.; Koo, B.; Chattopadhyay, S.; Shenchenko, E. V.; Talapin, D. V. Surface Functionalization of Semiconductor and Oxide Nanocrystals with Small Inorganic Oxoanions (PO_4^{3-}, MoO_4^{2-}) And Polyoxometalate Ligands. *ACS Nano* **2014**, *8*, 9388−9402.
(26) Llordés, A.; Hammack, A. T.; Buonsanti, R.; Tangirala, R.; Aloni, S.; Helms, B. A.; Milliron, D. J. Polyoxometalates and Colloidal Nanocrystals as Building Blocks for Metal Oxide Nanocomposite Films. *J. Mater. Chem.* **2011**, *21*, 11631−11638.
(27) Duong, J. T.; Bailey, M. J.; Pick, T. E.; McBride, P. M.; Rosen, E. L.; Buonsanti, R.; Milliron, D. J.; Helms, B. A. Efficient Polymer Passivation of Ligand-Stripped Nanocrystal Surfaces. *J. Polym. Sci., Part A: Polym. Chem.* **2012**, *50*, 3719−3727.
(28) Bailey, M. J.; van der Weegen, R.; Klemm, P. J.; Baker, S. L.; Helms, B. A. Stealth Rare Earth Oxide Nanodiscs for Magnetic Resonance Imaging. *Adv. Healthcare Mater.* **2012**, *1*, 437−442.
(29) Mendelsberg, R. J.; McBride, P. M.; Duong, J. T.; Bailey, M. J.; Llordés, A.; Milliron, D. J.; Helms, B. A. Dispersible Plasmonic Doped Metal Oxide Nanocrystal Sensors That Optically Track Redox Reactions in Aqueous Media with Single-Electron Sensitivity. *Adv. Opt. Mater.* **2015**, *3*, 1293−1300.
(30) Susumu, K.; Oh, E.; Delehanty, J. B.; Pinaud, F.; Gemmill, K. B.; Walper, S.; Breger, J.; Schroeder, M. J.; Stewart, M. H.; Jain, V.; et al. A New Family of Pyridine-Appended Multidentate Polymers as Hydrophilic Surface Ligands for Preparing Stable Biocompatible Quantum Dots. *Chem. Mater.* **2014**, *26*, 5327−5344.
(31) Palui, G.; Na, H. B.; Mattoussi, H. Poly(Ethylene Glycol)-Based Multidentate Oligomers for Biocompatible Semiconductor and Gold Nanocrystals. *Langmuir* **2012**, *28*, 2761−2772.
(32) Guhrenz, C.; Sayevich, V.; Weigert, F.; Hollinger, E.; Reichhelm, A.; Resch-Genger, U.; Gaponik, N.; Eychmüller, A. Transfer of Inorganic-Capped Nanocrystals Into Aqueous Media. *J. Phys. Chem. Lett.* **2017**, *8*, 5573−5578.
(33) Na, H.-K.; Kim, H.; Son, J. G.; Lee, J. H.; Kim, J.-K.; Park, J.; Lee, T. G. Facile Synthesis and Direct Characterization of Surface-Charge-Controlled Magnetic Iron Oxide Nanoparticles and Their Role in Gene Transfection in Human Leukemic T Cell. *Appl. Surf. Sci.* **2019**, *483*, 1069−1080.
(34) Schwabacher, J. C.; Kodaimati, M. S.; Weiss, E. A. Origin of the pH Dependence of Emission of Aqueous Dihydrolipoic Acid-Capped PbS Quantum Dots. *J. Phys. Chem. C* **2019**, *123*, 17574−17579.

https://dx.doi.org/10.1021/acs.chemmater.0c02399
Chem. Mater. 2020, 32, 8401−8411

(35) Dragoman, R. M.; Grogg, M.; Bodnarchuk, M. I.; Tiefenboeck, P.; Hilvert, D.; Dirin, D. N.; Kovalenko, M. V. Surface-Engineered Cationic Nanocrystals Stable in Biological Buffers and High Ionic Strength Solutions. *Chem. Mater.* **2017**, *29*, 9416−9428.
(36) Llordés, A.; Garcia, G.; Gazquez, J.; Milliron, D. J. Tunable Near-Infrared and Visible-Light Transmittance in Nanocrystal-in-Glass Composites. *Nature* **2013**, *500*, 323−326.
(37) Llordés, A.; Wang, Y.; Fernandez-Martinez, A.; Xiao, P.; Lee, T.; Poulain, A.; Zandi, O.; Saez Cabezas, C. A.; Henkelman, G.; Milliron, D. J. Linear Topology in Amorphous Metal Oxide Electrochromic Networks Obtained via Low-Temperature Solution Processing. *Nat. Mater.* **2016**, *15*, 1267−1273.
(38) Palui, G.; Aldeek, F.; Wang, W.; Mattoussi, H. Strategies for Interfacing Inorganic Nanocrystals with Biological Systems Based on Polymer-Coating. *Chem. Soc. Rev.* **2015**, *44*, 193−227.
(39) Du, L.; Wang, W.; Zhang, C.; Jin, Z.; Palui, G.; Mattoussi, H. A Versatile Coordinating Ligand for Coating Semiconductor, Metal, and Metal Oxide Nanocrystals. *Chem. Mater.* **2018**, *30*, 7269−7279.
(40) Wang, W.; Mattoussi, H. Engineering the Bio-Nano Interface Using a Multifunctional Coordinating Polymer Coating. *Acc. Chem. Res.* **2020**, *53*, 1124−1138.
(41) DeLongchamp, D. M.; Hammond, P. T. Highly Ion Conductive Poly(Ethylene Oxide)-Based Solid Polymer Electrolytes From Hydrogen Bonding Layer-by-Layer Assembly. *Langmuir* **2004**, *20*, 5403−5411.
(42) An, S. Y.; Jeong, I. C.; Won, M.-S.; Jeong, E. D.; Shim, Y.-B. Effect of Additives in PEO/PAA/PMAA Composite Solid Polymer Electrolytes on the Ionic Conductivity and Li Ion Battery Performance. *J. Appl. Electrochem.* **2009**, *39*, 1573−1578.
(43) Xue, Z.; He, D.; Xie, X. Poly(Ethylene Oxide)-Based Electrolytes for Lithium-Ion Batteries. *J. Mater. Chem. A* **2015**, *3*, 19218−19253.
(44) Nguyen, C. A.; Argun, A. A.; Hammond, P. T.; Lu, X.; Lee, P. S. Layer-by-Layer Assembled Solid Polymer Electrolyte for Electrochromic Devices. *Chem. Mater.* **2011**, *23*, 2142−2149.
(45) Barile, C. J.; Slotcavage, D. J.; McGehee, M. D. Polymer-Nanoparticle Electrochromic Materials that Selectively Modulate Visible and Near-Infrared Light. *Chem. Mater.* **2016**, *28*, 1439−1445.
(46) Ratautaite, V.; Bagdziunas, G.; Ramanavicius, A.; Ramanaviciene, A. An Application of Conducting Polymer Polypyrrole for the Design of Electrochromic pH and CO_2 sensors. *J. Electrochem. Soc.* **2019**, *166*, B297−B303.
(47) Deshmukh, M. A.; Gicevicius, M.; Ramanaviciene, A.; Shirsat, M. D.; Viter, R.; Ramanavicius, A. Hybrid Electrochemical/Electrochromic Cu(II) Ion Sensor Prototype Based on PANI/ITO-Electrode. *Sens. Actuators, B* **2017**, *248*, 527−535.
(48) Wirth, D. M.; Waldman, L. J.; Petty, M.; LeBlanc, G. Polyaniline Electrodeposition on Flexible ITO Substrates and the Effect of Curved Electrochemical Conditions. *J. Electrochem. Soc.* **2019**, *166*, D635−D637.
(49) Buonsanti, R.; Pick, T. E.; Krins, N.; Richardson, T. J.; Helms, B. A.; Milliron, D. J. Assembly of Ligand-Stripped Nanocrystals into Precisely Controlled Mesoporous Architectures. *Nano Lett.* **2012**, *12*, 3872−3877.
(50) Su, Y.-L.; Wang, J.; Liu, H.-Z. FTIR Spectroscopic Study on Effects of Temperature and Polymer Composition on the Structural Properties of PEO-PPO-PEO Block Copolymer Micelles. *Langmuir* **2002**, *18*, 5370−5374.
(51) Dong, J.; Ozaki, Y.; Nakashima, K. Infrared, Raman, and Near-Infrared Spectroscopic Evidence for the Coexistence of Various Hydrogen-Bond Forms in Poly(Acrylic Acid). *Macromolecules* **1997**, *30*, 1111−1117.
(52) Kirwan, L. J.; Fawell, P. D.; van Bronswijk, W. In Situ FTIR-ATR Examination of Poly(Acrylic Acid) Adsorbed Onto Hematite at Low pH. *Langmuir* **2003**, *19*, 5802−5807.
(53) Bronstein, L. M.; Huang, X.; Retrum, J.; Schmucker, A.; Pink, M.; Stein, B. D.; Dragnea, B. Influence of Iron Oleate Complex Structure on Iron Oxide Nanoparticle Formation. *Chem. Mater.* **2007**, *19*, 3624−3632.
(54) Gabka, G.; Leniarska, K.; Ostrowski, A.; Malinowska, K.; Skorka, L.; Donten, M.; Bujak, P. Effect of Indium Precursor and Ligand Type on the Structure, Morphology and Surface Functionalization of InP Nanocrystals Prepared by Gas−Liquid Approach. *Synth. Met.* **2014**, *187*, 94−101.
(55) Cho, S. H.; Ghosh, S.; Berkson, Z. J.; Hachtel, J. A.; Shi, J.; Zhao, X.; Reimnitz, L. C.; Dahlman, C. J.; Ho, Y.; Yang, A.; Liu, Y.; Idrobo, J.-C.; Chmelka, B. F.; Milliron, D. J. Syntheses of Colloidal F:In_2O_3 Cubes: Fluorine-Induced Faceting and Infrared Plasmonic Response. *Chem. Mater.* **2019**, *31*, 2661−2676.
(56) Pramanik, N. C.; Das, S.; Biswas, P. K. The Effect of Sn(IV) on Transformation of Co-Precipitated Hydrated In(III) and Sn(IV) Hydroxides to Indium Tin Oxide (ITO) Powder. *Mater. Lett.* **2002**, *56*, 671−679.
(57) Su, C.; Suarez, D. L. Coordination of Adsorbed Boron: a FTIR Spectroscopic Study. *Environ. Sci. Technol.* **1995**, *29*, 302−311.
(58) Jun, L.; Shuping, X.; Shiyang, G. FT-IR and Raman Spectroscopic Study of Hydrated Borates. *Spectrochim. Acta, Part A* **1995**, *51*, 519−532.
(59) Peak, D.; Luther, G. W., III; Sparks, D. L. ATR-FTIR Spectroscopic Studies of Boric Acid Adsorption on Hydrous Ferric Oxide. *Geochim. Cosmochim. Acta* **2003**, *67*, 2551−2560.
(60) Owen, B. B. The Dissociation Constant of Boric Acid From 10 to 50°. *J. Am. Chem. Soc.* **1934**, *56*, 1695−1967.
(61) zum Felde, U.; Haase, M.; Weller, H. Electrochromism of Highly Doped Nanocrystalline SnO_2:Sb. *J. Phys. Chem. B* **2000**, *104*, 9388−9395.
(62) Agrawal, A.; Johns, R. W.; Milliron, D. J. Control of Localized Surface Plasmon Resonances in Metal Oxide Nanocrystals. *Annu. Rev. Mater. Res.* **2017**, *47*, 1−31.
(63) Pattathil, P.; Giannuzzi, R.; Manca, M. Self-Powered NIR-Selective Dynamic Windows Based on Broad Tuning of the Localized Surface Plasmon Resonance in Mesoporous ITO Electrodes. *Nano Energy* **2016**, *30*, 242−251.
(64) Williams, T. E.; Chang, C. M.; Rosen, E. L.; Garcia, G.; Runnerstrom, E. L.; Williams, B. L.; Koo, B.; Buonsanti, R.; Milliron, D. J.; Helms, B. A. NIR-Selective Electrochromic Heteromaterial Frameworks: a Platform to Understand Mesoscale Transport Phenomena in Solid-State Electrochemical Devices. *J. Mater. Chem. C* **2014**, *2*, 3328−3328.
(65) Thoniyot, P.; Tan, M. J.; Karim, A. A.; Young, D. J.; Loh, X. J. Nanoparticle-Hydrogel Composites: Concept, Design, and Applications of These Promising, Multi-Functional Materials. *Adv. Sci.* **2015**, *2*, 1400010−1400013.
(66) Karg, M.; Pich, A.; Hellweg, T.; Hoare, T.; Lyon, L. A.; Crassous, J. J.; Suzuki, D.; Gumerov, R. A.; Schneider, S.; Potemkin, I. I.; Richtering, W. Nanogels and Microgels: From Model Colloids to Applications, Recent Developments, and Future Trends. *Langmuir* **2019**, *35*, 6231−6255.
(67) Cheng, C.; Zhang, C.; Wang, D. Using Hydrogel to Diversify the Adaptability and Applicability of Functional Nanoparticles: From Nanotech-Flavored Jellies to Artificial Enzymes. *Langmuir* **2019**, *35*, 8612−8628.
(68) Cheng, H.; Lin, S.; Muhammad, F.; Lin, Y.-W.; Wei, H. Rationally Modulate the Oxidase-Like Activity of Nanoceria for Self-Regulated Bioassays. *ACS Sens.* **2016**, *1*, 1336−1343.
(69) Kang, T.; Kim, Y. G.; Kim, D.; Hyeon, T. Inorganic Nanoparticles with Enzyme-Mimetic Activities for Biomedical Applications. *Coord. Chem. Rev.* **2020**, *403*, 213092.
(70) Saleh, N. B.; Milliron, D. J.; Aich, N.; Katz, L. E.; Liljestrand, H. M.; Kirisits, M. J. Importance of Doping, Dopant Distribution, and Defects on Electronic Band Structure Alteration of Metal Oxide Nanoparticles: Implications for Reactive Oxygen Species. *Sci. Total Environ.* **2016**, *568*, 926−932.
(71) Wehmas, L. C.; Anders, C.; Chess, J.; Punnoose, A.; Pereira, C. B.; Greenwood, J. A.; Tanguay, R. L. Comparative Metal Oxide Nanoparticle Toxicity Using Embryonic Zebrafish. *Toxicol. Rep.* **2015**, *2*, 702−715.

https://dx.doi.org/10.1021/acs.chemmater.0c02399
Chem. Mater. 2020, 32, 8401−8411

(72) Deline, A. R.; Nason, J. A. Evaluation of Labeling Methods Used for Investigating the Environmental Behavior and Toxicity of Metal Oxide Nanoparticles. *Environ. Sci.: Nano* **2019**, *6*, 1043−1066.
(73) Bhattacharya, P.; Neogi, S. Antibacterial Properties of Doped Nanoparticles. *Rev. Chem. Eng.* **2019**, *35*, 861−876.

https://dx.doi.org/10.1021/acs.chemmater.0c02399
Chem. Mater. 2020, 32, 8401−8411